Thomson scattering diagnostics of nonthermal plasma from particle-in-cell simulations

Audrey Farrell
University of California, Los Angeles
Los Angeles, California
audfarrell@g.ucla.edu

Chaojie Zhang
University of California, Los Angeles
Los Angeles, California

Yipeng Wu University of California, Los Angeles Los Angeles, California

Zan Nie
University of California, Los Angeles
Los Angeles, California

Noa Nambu
University of California, Los Angeles
Los Angeles, California

Mitchell Sinclair
University of California, Los Angeles
Los Angeles, California

Kenneth Marsh
University of California, Los Angeles
Los Angeles, California

Chandrasekhar Joshi
University of California, Los Angeles
Los Angeles, California

Abstract-Optical Thomson scattering is now a mature diagnostic tool for precisely measuring local plasma density and temperature. These measurements typically take advantage of a simplified analytical model of the scattered spectrum, which is built upon the assumption that each plasma species is in thermal equilibrium. However, this assumption fails for most laboratory plasmas of interest, which are often produced through high field ionization of atoms via ultrashort laser pulses and vulnerable to several kinetic instabilities. While it is possible to analytically model the Thomson scattered spectrum for some non-Maxwellian distribution functions, it is often not practical to do so for laboratory plasmas with highly complex and unstable distribution functions. We present a new method for predicting the Thomson scattered spectrum from any plasma directly from fully kinetic particle-in-cell simulations. This approach allows us to model the contributions of kinetic instabilities to the Thomson spectrum that aren't taken into account in Maxwellian theory. We demonstrate this method's capability to capture nonthermal features in the Thomson spectrum by simulating a simple bumpon-tail plasma as well as a more complex laser-ionized plasma. The versatility of this approach makes it an effective aid in the experimental design of Thomson diagnostics to directly characterize kinetic instabilities in laboratory plasmas.

Index Terms—plasma measurement, low-temperature plasmas, plasma diagnostics, plasma simulation, plasma stability, plasma density, plasma temperature

I. Introduction

Accurate information about the phase-space of laboratory plasmas is essential for applications in wakefield acceleration, fusion science, radiation generation, and laboratory astrophysics. Such plasmas are often in a nonthermal state - that is to say that the plasma electrons and ions have velocity distribution functions that are non-Maxwellian and/or

This material is based upon work supported by the National Science Foundation under Grant Nos. 2034835 and 2003354, and the U.S. Department of Energy under Grant Nos. DE-SC0010064 and DE-SC0014043.

anisotropic. These plasmas eventually reach thermal equilibrium through collisions and self-organization via collisionless kinetic instabilities. Experimentally, it is important to develop techniques that will provide time resolved information about the evolution of the phase space of the plasma species. For decades Thomson scattering has been used for local density, temperature, and drift velocities in laboratory plasmas [1]. More recently, the advent of ultrashort laser pulses has allowed for the direct measurement of evolution in the Thomson spectrum [2]. However, most applications of Thomson scattering rely on the assumption of stable, linear plasma in thermal equilibrium, and previous theoretical work has shown that even small deviations from Maxwellian electron velocity distribution (EVD) functions can lead to significant error in the Thomson scattered spectra predicted by Maxwellian theory [3]–[5].

Nonequilibrium plasmas are susceptible to many kinetic instabilities that will impact the collective Thomson scattering of a laser beam [6], [7]. While it is possible to analytically model the Thomson spectrum from many non-Maxwellian EVDs [3]–[5], [8], doing so is often very complex, and not necessarily practical when planning an experiment or analyzing existing data, particularly for laboratory plasmas with complex EVDs. We present an alternative method for predicting the Thomson scattered spectra using kinetic particle-in-cell (PIC) simulations of laboratory plasmas. This method is independent of the plasma itself, instead depending on the fundamental definition of Thomson scattering in order to provide a general method that can be used to optimize scattering geometries that directly probe nonlinear and nonthermal plasma waves of interest in a given experiment.

II. FUNDAMENTALS OF THOMSON SCATTERING

At its core, Thomson scattering is a three wave interaction between a low energy probe, electron plasma waves present in the plasma, and scattered photons. This is expressed in the phase matching conditions

$$\mathbf{k}_0 = \mathbf{k}_s + \mathbf{k}_m \tag{1}$$

$$\omega_0 = \omega_s + \omega_m \tag{2}$$

where (k_0, ω_0) are the wavevector and frequency of the incident probe, (k_s, ω_s) are the wavevector and frequency of the scattered light, and (k_m, ω_m) are the wavevector and frequency of the measured electron plasma wave, respectively. Fig. 1a illustrates these phase matching conditions geometrically as parallelograms connecting the EM wave and electron plasma wave dispersion relations. The red parallelogram demonstrates scattering off of plasma waves traveling to the left (k_l, ω_l) , resulting in redshifted light at (k_{sl}, ω_{sl}) . Similarly the blue parallelogram demonstrates scattering from plasma waves traveling to the right (k_r, ω_r) , resulting in blueshifted light (k_{sr}, ω_{sr}) . The resonant plasma oscillations produce corresponding peaks in the Thomson spectrum, as illustrated in Fig. 1b.

For Maxwellian plasmas, the Thomson scattered spectrum has an analytical form factor given by the spectral density function (SDF) $S(\boldsymbol{k},\omega)$

$$S(\mathbf{k}, \omega) \equiv \lim_{V \to \infty, T \to \infty} \frac{1}{VT} \left\langle \frac{|n_e(\mathbf{k}, \omega)|^2}{n_{e0}} \right\rangle$$
(3)

$$= \frac{2\pi}{k} \left[\left| 1 - \frac{\chi_e}{\epsilon} \right|^2 f_e \left(\frac{\omega}{k} \right) + Z_i \left| \frac{\chi_e}{\epsilon} \right|^2 f_i \left(\frac{\omega}{k} \right) \right] \tag{4}$$

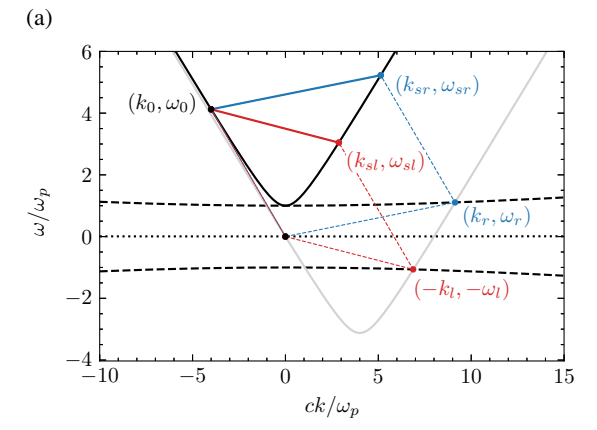
where V is the scattering volume, T is the scattering time, n_{e0} is the mean electron density, χ_e is the electron susceptibility, ϵ is the permittivity, Z_i is the ion charge, and $f_e(v)$, $f_i(v)$ are the electron and ion velocity distribution functions, respectively.

III. EXTRACTING THOMSON SPECTRA FROM SIMULATION

By applying this geometric understanding of the Thomson scattered spectrum to simulated density fluctuations, we can predict the spectra of any simulated plasma.

A. Simulations in One Dimension

In 1D simulations, we only have information about the plasma along one axis, and so we take the simulated axis as parallel to the probed electron plasma wave, (k_m, ω_m) . We model the dispersion relation of the electron plasma waves by taking the spatiotemporal fast Fourier transform (FFT) of the simulated electron density $n_e(x_{\parallel},t)$, which gives a map of the amplitudes of plasma oscillations in (k,ω) -space. Fig. 2a shows this dispersion space for a Maxwellian plasma, where the simulation closely follows the theoretical dispersion relations for Bohm-Gross and ion-acoustic waves, as expected. For the chosen scattering geometry and plasma parameters, the Thomson scattering parameter $\alpha=1/k\lambda_D$ for this simulation is 2.8, meaning that we are in the highly collective regime,



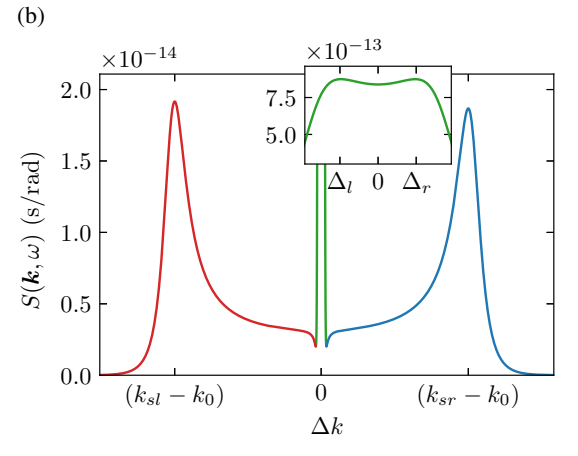


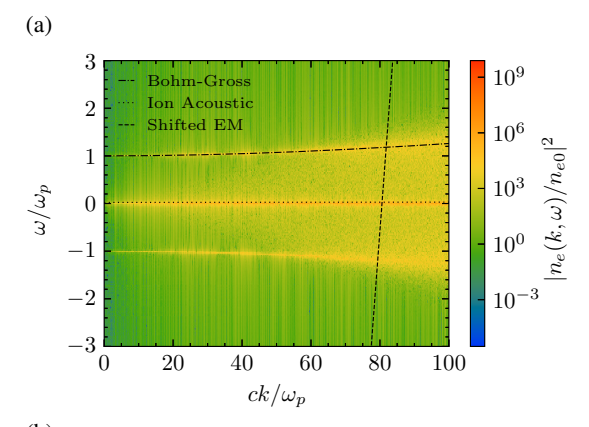
Fig. 1: (a) Demonstration of the phase matching conditions for Thomson scattering in a thermal plasma. The incident probe (\mathbf{k}_0,ω_0) and scattered light (\mathbf{k}_s,ω_s) follow the dispersion relation for electromagnetic waves in plasma, $\omega^2=\omega_p^2+c^2k^2$, shown in solid black. The grey curve shows the shifted EM wave dispersion relation as written in (5). The electron plasma waves are approximated as Bohm-Gross waves (dashed black curve) and ion-acoustic waves (dotted black curve). The red and blue parallelograms demonstrate the phase-matching conditions for the up- and downshifted peaks in the Thomson scattered spectrum shown in (b). The green feature in (b) is the ion feature produced through scattering off of ion-acoustic waves in the plasma, with peaks at the ion-acoustic matching conditions $\Delta k = \Delta_{l,r}$ close to zero, shown in detail on the inset plot.

and expect to see distinct features in the Thomson spectrum corresponding to Bohm-Gross and ion-acoustic waves.

If we shift the electromagnetic (EM) wave dispersion relation such that $(k_{0\parallel},\omega_0)$ sits at the origin, as shown by the grey curve in Fig. 1a, the set of (k_{\parallel},ω) along that curve are those that satisfy the phase-matching conditions in (1) and (2). Explicitly, we take the (k_m,ω_m) given by

$$\omega_m = \sqrt{w_p^2 + c^2(k_m - k_{\parallel 0})^2 + c^2k_{\perp 0}^2} - w_0$$
 (5)

where $k_{\parallel 0}$ and $k_{\perp 0}$ are the projections of the probe wavevector



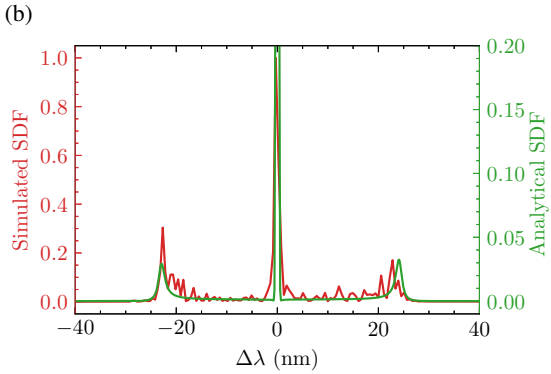


Fig. 2: (a) $|n_e(k_\parallel,\omega)|^2$ for a 1D OSIRIS simulation of a 10eV, $n_e=10^{18} {\rm cm}^{-3}$ Maxwellian plasma. Theoretical curves for Bohm-Gross, ion-acoustic, and electromagnetic wave dispersion relations are shown for the given plama parameters, where the EM wave dispersion relation has been shifted such that $(k_{0\parallel},\omega_0)$ sits on the origin as given in (5). The Thomson spectrum is extracted underneath this shifted dispersion relation to satisfy the phase matching conditions. (b) Simulated (red) and analytical (green) Thomson spectra for an 800nm probe scattering at $\theta=150^\circ$, each normalized to their maximum.

onto the \hat{k}_m axis. Taking $|n_e(k_\parallel,\omega)|^2$ at these points maps directly to intensity of the Thomson scattered spectrum, as shown in Fig. 2b. With this method we are able to calculate a similar form factor to the analytical $S(\mathbf{k},\omega)$ for Maxwellian plasma given in (4).

B. Simulations in Two Dimensions

The core principle of this method is the same in two dimensions as in one. The primary complication is a computational one: in 1D simulations we must treat the simulated axis as the probed axis in our scattering geometry, but in 2D we have enough information to extract the Thomson spectrum for any scattering geometry in the plane of the simulation. For high resolution simulations in 2D, extracting the Thomson spectrum in exactly the same way as in 1D would require holding the entire simulation at all time steps in computer memory at once, which is typically not possible due to hardware limitations.

For the purpose of extracting the Thomson spectrum, we only care about $n_e(k_\parallel,\omega)$ near the probed (k_m,ω_m) . Since we typically set $\Delta x_\parallel \approx 0.2/k_m$ in order to spatially resolve the plasma wave we're interested in, the maximum k_\parallel simulated is typically $k_\parallel, \max \gtrsim 5k_m$, which is significantly higher than anything we need to calculate the Thomson spectrum. We can perform the spatial FFT while iteratively loading each time step in the simulation, and immediately crop to only the k_\parallel -range necessary to extract the Thomson spectrum before moving forward. This reduces the amount of data we need to store in memory simultaneously, allowing us to analyze high resolution simulations while maintaining individual contributions to the scattered spectrum from each x_\perp -position in the plasma.

A step-by-step overview of this analysis is as follows:

- 1) For each time step t_i :
 - a) Load the full array of local densities, $n_e(x, y, t_i)$
 - b) Rotate $n_e(x, y, t_i)$ to align with the probed \hat{k}_m , giving $n_e(x_{\parallel}, x_{\perp}, t_i)$
 - c) Take the FFT of $n_e(x_\parallel,x_\perp,t_i)$ along the \hat{x}_\parallel axis, giving $n_e(k_\parallel,x_\perp,t_i)$
 - d) Clip $n_e(k_\parallel, x_\perp, t_i)$ to the maximum k_\parallel needed to define the Thomson spectrum for this simulation.
- 2) Take the FFT of the clipped $n_e(k_{\parallel}, x_{\perp}, t)$ along the t-axis, giving $n_e(k_{\parallel}, x_{\perp}, \omega)$
- 3) Take the sum of $|n_e(k_{\parallel}, x_{\perp}, \omega)|^2$ along the x_{\perp} -axis, giving $|n_e(k_{\parallel}, \omega)|^2$
- 4) Extract the Thomson spectrum along the shifted EM wave dispersion relation as given in (5).

C. Boundary Conditions

This analysis depends heavily on the discrete Fourier transform, which assumes periodic boundary conditions in x_{\parallel} and t. In most cases this is not true, and we need to remove edge artifacts from the final $n_e(k_{\parallel},\omega)$ spectrum that arise from the discontinuous boundaries of the simulation. To do so we use periodic plus smooth (P+S) decomposition of $n_e(x_{\parallel},t)$. P+S breaks the data into a periodic component (containing the spectrum we're interested in) and a smooth component that resolves the discontinuities on the edges of the data. This method preserves the spectral information in the data better than traditional methods of removing edge artifacts [9].

In 2D simulations, a conventional P+S approach would again require loading the entire simulation at once in order to calculate the boundary discontinuities for $n_e(x_\parallel,t)$ at each x_\perp position before taking the Fourier transform. To work around this we instead enforce that the density drops to zero on the edges of the x_\perp -axis. This allows us to calculate the boundary discontinuities using only the first and last timesteps of the simulation. We then calculate the smooth component of $n_e(x_\parallel,t)$ for all x_\perp at once, and then subtract this component from $n_e(k_\parallel,x_\perp,\omega)$ as calculated in the previous section.

D. Finite Probe Beams

The example in Fig. 2b was calculated for a perfectly monochromatic probe beam, but in reality the bandwidth of

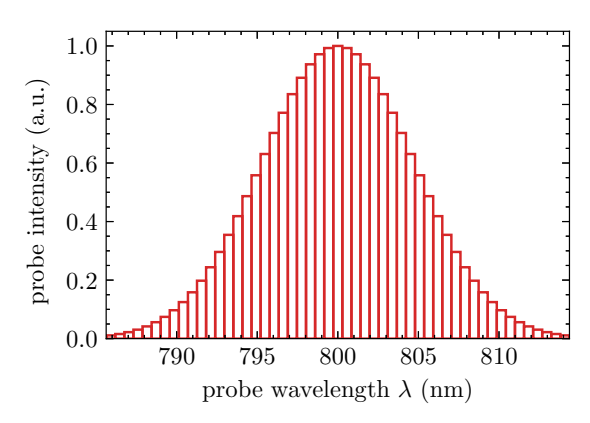


Fig. 3: Discretized spectrum of an 800nm probe beam with 5nm bandwidth.

the probe beam will broaden the Thomson spectrum. To take this into account we discretize the probe spectrum, as shown in Fig. 3, and take $S_{tot}(\boldsymbol{k},\omega,\lambda_0,\Delta\lambda) = \sum_j I_j S_j(\boldsymbol{k},\omega,\lambda_j)$ where I_j is the normalized intensity of a single wavelength in the probe spectrum.

Currently the temporal profile of the probe is not taken into account and the Thomson spectra are calculated using the full temporal range of the simulation. Shorter scattering time corresponds to lower resolution in ω , so while it is possible to model the ultrashort probes used for time-resolved Thomson scattering measurements, care needs to be taken in maintaining high enough spectral resolution for this analysis. Similarly the spatial intensity profile of the probe beam is not currently included in this analysis, so all locations within the simulation box are considered equal contributors to the Thomson spectrum. Future work will focus on including these finite probe effects in the extracted spectra.

IV. BUMP ON TAIL PLASMA

To test the capability of this method to model Thomson scattering from unstable plasma, we simulated a bump-ontail plasma in 1D OSIRIS. Fig. 4 shows the electron velocity distribution consisting of a main population of stationary 10eV electrons at $n_{0,\mathrm{main}} = 10^{18}\mathrm{cm}^{-3}$ and a beam of 10eV electrons streaming at 0.02c with $n_{0,\mathrm{beam}} = 10^{17}\mathrm{cm}^{-3}$. The bump in the EVDF will excite an unstable plasma wave that grows nonlinearly as the plasma approaches thermal equilibrium. The full dispersion relation for this asymmetric two-stream instability (ATSI) was solved numerically for this plasma using Xie et al.'s PDRK code [10]. Fig. 5a demonstrates that the maximum growth rate calculated (green) matches the growth of corresponding density fluctuations in the simulation (red).

Fig. 5b shows the dispersion space for this simulation alongside the theoretical curve for 10eV Bohm-Gross waves at $n_{e0} = n_{0,\mathrm{main}} + n_{0,\mathrm{beam}}$ (black dash-dotted line) and the calculated real frequency of the asymmetric streaming instability (blue dashed line). The shifted EM wave dispersion relation shown is for an 800nm probe beam with a 90° scattering angle. The dispersion space for this plasma is highly

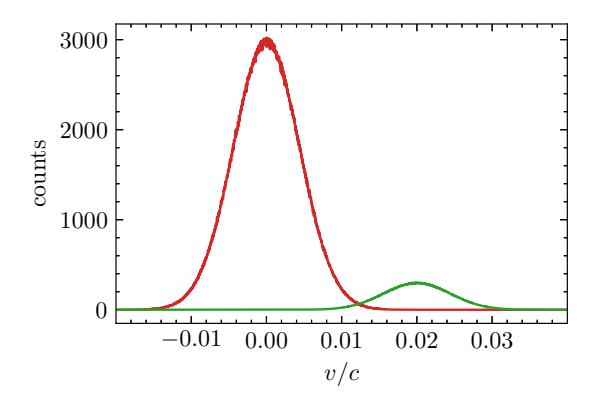


Fig. 4: Electron velocity distribution for a bump on tail plasma initialized in 1D OSIRIS. The plasma consists of a 10eV population with $n_e=10^{18} {\rm cm}^{-3}$ (red) and a 10eV, $n_e=10^{17} {\rm cm}^{-3}$ beam streaming with a velocity of 0.02c (green).

asymmetric about $\omega=0$, resulting in an asymmetric Thomson spectrum, as seen in Fig. 5c.

In addition to this asymmetry, the calculated Thomson spectrum has a frequency shift between electron features that cannot be reproduced using the Maxwellian model of Thomson scattering (shown in green in Fig. 5c). The expression in (4) doesn't take into account non-thermal electron plasma waves such as ATSI, and so fails to predict the spectrum for the bump-on-tail plasma even though both electron populations are Maxwellian. A similar distribution is discussed at length in [6], where a similar Thomson spectrum is numerically calculated by directly solving the wave equation of the scattered waves.

V. LASER-IONIZED PLASMA

While the bump-on-tail plasma of the previous section does well to highlight the impact of instabilities on the Thomson spectrum, it is far from a realistic laboratory plasma. We simulated the laser-ionization of neutral helium in 2D OSIRIS. An 8mJ, 50fs, 800nm ($a_0=0.273$) linearly polarized laser pulse was sent through $n_0=5\cdot 10^{18} {\rm cm}^{-3}$ of neutral helium with a short (2.5µm) linear up- and downramp in density along the pump axis. The simulation ran for just over 3ps. We define an 800nm probe beam with 5nm bandwidth incident perpendicular to the pump beam and a scattering angle of 150° . Fig. 6a shows the electron density immediately after the pump has left the simulation box, along with the probed k_m direction for this scattering geometry (105° relative to the pump axis).

Calculating $|n_e(k_{\parallel},\omega)|^2$ as outlined in Section III-B for all timesteps after the pump has left, we once again see a dispersion relation that is far from thermal, shown in Fig. 6b. We can see features close to a 100eV Bohm-Gross dispersion relation at low k, but around the shifted EM wave dispersion relation (shown here in white) the spectrum is dominated by asymmetric blobs arising from higher order kinetic effects. Fig. 6c shows the extracted Thomson spectrum for this simulation (red) alongside the theoretical spectrum for a 100eV

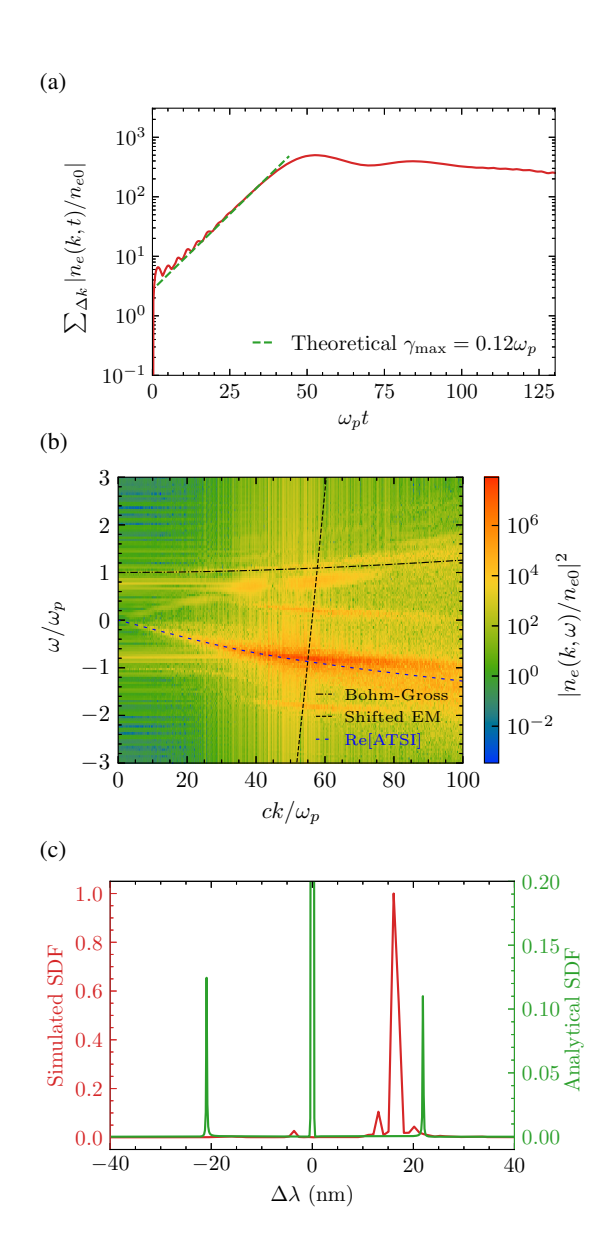


Fig. 5: (a) Simulated (red) evolution of density fluctuations in the bump-on-tail plasma over time for the fastest growing spatial frequency, $k_{\rm max}\approx (57\pm 2)\omega_p/c$. The green dashed line shows the maximum growth rate predicted by kinetic theory. (b) $|n_e(k_\parallel,\omega)|^2$ for a 1D OSIRIS simulation of a the bump-on-tail plasma. The shifted EM and Bohm-Gross dispersion relations are shown in black. The blue curve shows the real frequencies of the asymmetric two-stream instability, calculated numerically using the PDRK code in [10]. (c) Simulated (red) and analytical (green) Thomson spectra for an 800nm probe scattering at $\theta=90^\circ$, each normalized to their maximum.

Maxwellian plasma. Note that this simulation did not include ions after ionization, and so we do not expect to see ionacoustic features in the simulated spectrum. Most notably, the electron features in the simulated spectrum do not occur at the same frequency shift as the Maxwellian spectrum even though the plasma densities are the same.

This simulation was modelled after experimental conditions in [2], where the measured Thomson spectrum also showed electron features at frequency shifts below ω_p for the known plasma density.

VI. CONCLUSION

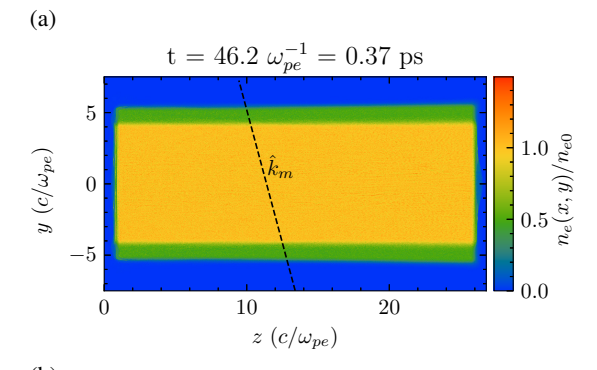
We have presented a computational method for predicting the Thomson scattered spectrum from plasmas simulated in kinetic particle-in-cell codes. This method can be applied to any 1D or 2D simulation regardless of the electron distribution function, allowing us to predict the Thomson spectrum for nonthermal and unstable plasmas. This method is capable of reproducing the established theoretical spectrum for Maxwellian plasma, and can predict nonthermal features that the Maxwellian model cannot.

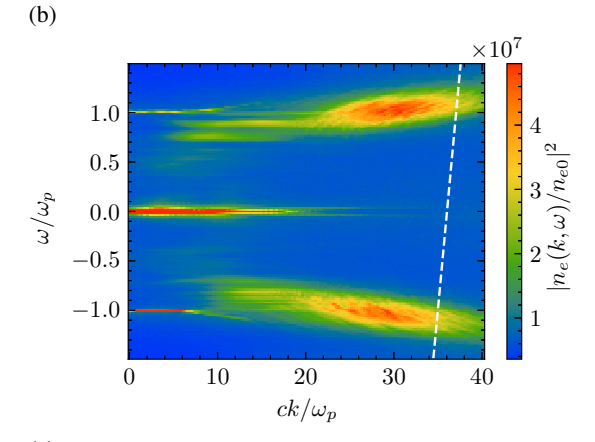
Simulating the Thomson spectrum from a 1D bump-on-tail plasma produces an asymmetric dispersion relation consistent with kinetic theory for asymmestric two-stream instability, and our method is able to show this asymmetry in the Thomson spectrum. Reproducing a laser-ionized helium plasma in 2D simulation shows asymmetric nonthermal features in the dispersion relation as well, and our method was capable of predicting a broad frequency spectrum with scattered frequencies from below ω_p to above ω_p , as seen in experimental measurements [2].

This method is particularly well suited for optimizing Thomson scattering diagnostics to directly probe kinetic instabilities in laboratory plasmas. One simulation of the experimental plasma conditions can be used to calculate the scattered spectrum for any scattering geometry and probe beam parameters, allowing for optimization of the experimental layout to target specific plasma waves of interest. Given that Thomson scattering diagnostics are nonperturbing and can give time-resolved spectra using ultrashort probes, this method provides a highly advantageous means of characterizing stability and nonthermal effects in laboratory plasmas.

REFERENCES

- D. H. Froula, S. H. Glenzer, N. C. Luhmann, and J. Sheffield, *Plasma Scattering of Electromagnetic Radiation: Theory and Measurement Techniques*, 2nd ed. Boston: Academic Press, 2011. [Online]. Available: https://www.sciencedirect.com/science/article/pii/B9780123748775000178
- [2] C. Zhang, C.-K. Huang, K. A. Marsh, C. E. Clayton, W. B. Mori, and C. Joshi, "Ultrafast optical field–ionized gases—a laboratory platform for studying kinetic plasma instabilities," *Science Advances*, vol. 5, no. 9, p. eaax4545, 2019. [Online]. Available: https://www.science.org/doi/abs/10.1126/sciadv.aax4545
- [3] A. L. Milder, S. T. Ivancic, J. P. Palastro, and D. H. Froula, "Impact of non-maxwellian electron velocity distribution functions on inferred plasma parameters in collective thomson scattering," *Physics of Plasmas*, vol. 26, no. 2, p. 022711, 2019. [Online]. Available: https://doi.org/10.1063/1.5085664
- [4] I. Abramovic, M. Salewski, and D. Moseev, "Collective thomson scattering model for arbitrarily drifting bi-maxwellian velocity distributions," *AIP Advances*, vol. 9, no. 3, p. 035252, 2019. [Online]. Available: https://doi.org/10.1063/1.5088949
- [5] R. J. Henchen, M. Sherlock, W. Rozmus, J. Katz, D. Cao, J. P. Palastro, and D. H. Froula, "Observation of nonlocal heat flux using thomson scattering," *Phys. Rev. Lett.*, vol. 121, p. 125001, Sep 2018. [Online]. Available: https://link.aps.org/doi/10.1103/PhysRevLett.121.125001





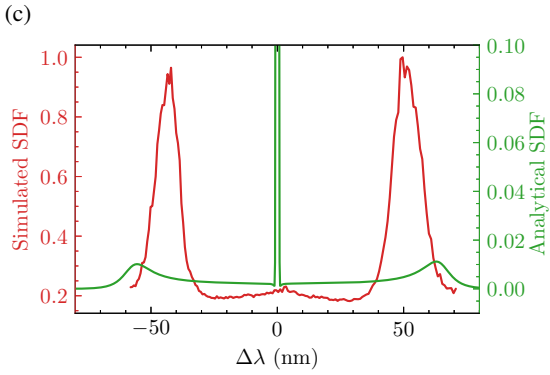


Fig. 6: (a) Simulated electron density of laser-ionized helium $(n_{e0}=5\cdot 10^{18} {\rm cm}^{-3})$ immediately after the pump beam (travelling from left to right) leaves the simulation box. The dashed line shows the direction of the probed plasma wavevector for a probe incident at 90° relative to the pump and a 150° scattering angle. (b) Simulated $|n_e(k_{\parallel},\omega)|^2$ for this simulation. The white dashed line shows the shifted EM dispersion relation given by (5) for an 800nm probe. (c) Calculated Thomson spectrum (red) from this simulation alongside the theoretical Thomson spectrum for a 100eV Maxwellian helium plasma (green).

[6] K. Sakai, S. Isayama, N. Bolouki, M. S. Habibi, Y. L. Liu, Y. H. Hsieh, H. H. Chu, J. Wang, S. H. Chen, T. Morita, K. Tomita, R. Yamazaki, Y. Sakawa, S. Matsukiyo, and Y. Kuramitsu, "Collective thomson scattering in non-equilibrium laser produced two-stream plasmas," *Physics of Plasmas*, vol. 27, no. 10, p. 103104, oct 2020. [Online].

- Available: https://doi.org/10.1063/5.0011935
- [7] C. Bruulsema, W. Rozmus, G. F. Swadling, S. Glenzer, H. S. Park, J. S. Ross, and F. Fiuza, "On the local measurement of electric currents and magnetic fields using thomson scattering in weibel-unstable plasmas," *Physics of Plasmas*, vol. 27, no. 5, p. 052104, 2020. [Online]. Available: https://doi.org/10.1063/1.5140674
- [8] J. Zheng, C. X. Yu, and Z. J. Zheng, "Effects of non-maxwellian (super-gaussian) electron velocity distribution on the spectrum of thomson scattering," *Physics of Plasmas*, vol. 4, no. 7, pp. 2736–2740, 1997. [Online]. Available: https://doi.org/10.1063/1.872141
- [9] L. Moisan, "Periodic plus smooth image decomposition," *Journal of Mathematical Imaging and Vision*, vol. 39, no. 2, pp. 161–179, Feb 2011. [Online]. Available: https://doi.org/10.1007/s10851-010-0227-1
- [10] H. Xie and Y. Xiao, "Pdrk: A general kinetic dispersion relation solver for magnetized plasma*," *Plasma Science and Technology*, vol. 18, no. 2, p. 97, feb 2016. [Online]. Available: https://dx.doi.org/10.1088/1009-0630/18/2/01